Waveform-Based Modeling and Characterization of Microwave Power Heterojunction Bipolar Transistors

Ce-Jun Wei, *Member, IEEE,* Y. Ellen Lan, *Member, IEEE,* James C. M. Hwang, *Fellow, IEEE,* Wu-Jing Ho, *Member, IEEE,* and J. Aiden Higgins, *Senior Member, IEEE*

***Abstract*—A waveform measurement technique has been successfully used to extract the large-signal nonlinear characteristics of microwave power heterojunction bipolar transistors. The extracted model parameters were compared to those extracted from dc and small-signal parameters in a conventional manner. It was found that, for high input drive conditions, the present model predicts a much longer collector transit time than the conventional model. Therefore, the present model is more consistent with the physical structure of the transistors and more suitable for evaluating future design improvement.**

I. INTRODUCTION

TRADITIONALLY, large-signal models of microwave transistors are extracted from dc I-V characteristics and bias-dependent small-signal S-parameters. The model is then verified against load-pull measurement data. This traditional approach often has several drawbacks: 1) discrepancy between dc and small-signal characteristics due to time-dependent trapping effects, 2) limited bias range of dc and small-signal data due to thermal and oscillation problems, 3) error in load-pull measurement, and 4) nonphysical model due to numerical optimization techniques. In comparison, time-domain waveforms under real operating conditions accurately reflect the transistor nonlinear characteristics [1]–[6]. Therefore, it is desirable to extract and verify a large-signal model based on the measured waveforms. Further, before such a technique is fully developed, it will be beneficial to refine the traditionally constructed large-signal models using the measured waveforms beside load-pull data. This is especially true when the large-signal model is harmonic-balance based, and the power amplifier design requires careful termination of harmonics.

Recently, the intrinsic nonlinear drain current source for a MESFET or MODFET has been extracted from the measured waveforms, assuming all other parametérs, such as the delay time, are known from bias-dependent S-parameters [7]. As for HBT's, the intrinsic base-emitter and base-collector waveforms of an HBT have been measured and compared to that predicted by a conventional model [8]. This paper expands on [8] by reporting a modified modeling and characterization technique in detail. In particular, the measured waveforms are directly used to extract the nonlinear characteristics of the intrinsic HBT junctions. The base-collector capacitances are allowed to vary with both the collector voltage and current, while the collector current source is made proportional to only the conductive part of the emitter current. A vector error-correction procedure is used, resulting in improved speed and accuracy.

Manuscript received March 1, 1995; revised July 10, 1995.

C. J. Wei, Y. E. Lan, and J. C. M. Hwang are with Lehigh University, Bethlehem, PA 18015 USA.

W. J. Ho and J. A. Higgins are with Rockwell International, Thousand Oaks, CA 91360 USA.

IEEE Log Number 9415465.

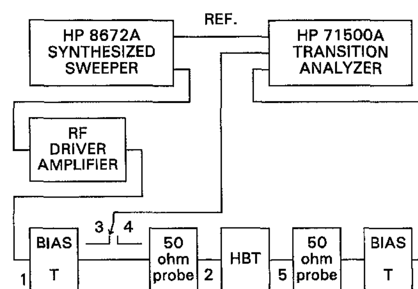

Fig. 1. Schematics of the waveform measurement setup. The HBT under test is contacted by a pair of 40 GHz wafer probes, followed by a pair of bias-T's. Broad-band couplers and switches are used to allow up to the seventh harmonic signals to be measured. An HP 71500A transition analyzer is used to measure the harmonic magnitudes and phases of the input, reflected and transmitted signals.

II. WAVEFORM CHARACTERIZATION TECHNIQUE

The waveform measurement set up is depicted in Fig. 1. An HP 71500A transition analyzer is used to measure the harmonic magnitudes and phases of the input, reflected and transmitted signals. Broad-band couplers and switches are used to allow up to the seventh harmonic signals to be included. The HBT is contacted by a pair of 40 GHz wafer probes, followed by a pair of bias-T's. The voltage waveforms measured by the transition analyzer are transformed to the voltage and current waveforms at the HBT, once the S-parameters of the input and output circuits are known. An HP 8510B network analyzer is used to characterize the input and output circuits. The overall calibration procedure is described next.

The present calibration procedure takes into account all the error terms, such as losses, leakages, and source and load mismatches. As shown in Fig. 2, the input of the incident coupler is designated Port 1, while the input of the HBT is designated Port 2. Port 3 is the output of the incident coupler. Port 4 is the output of the reflection coupler. On the output side, Port 5 is the output of the HBT, while Port 6 is the output of the second bias-T. The input circuit between Ports 1 and 2 can be described by a 4 × 4 scattering matrix S^{IN}, while the output circuit between Ports 5 and 6 can be described by a 2 × 2 scattering matrix S^{OUT}. Let a_I and b_I be the incident and reflected wave parameters at the Ith port. Assuming the inputs to the transition analyzer are perfectly matched, then

0018-9480/95$04.00 © 1995 IEEE

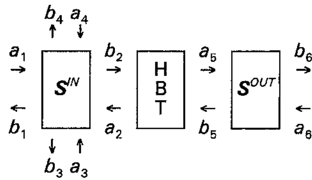

Fig. 2. S-parameter representation of the measurement setup. The voltage waveforms measured by the transition analyzer of Fig. 1 are transformed to the voltage and current waveforms at the HBT, once the S-parameters of the input and output circuits. $S^{\rm IN}$ and $S^{\rm OUT}$ are known.

$a_3 = a_4 = a_6 = 0$ and

$$b_1 = S_{11}a_1 + S_{12}a_2 \quad (1)$$
$$b_2 = S_{21}a_1 + S_{22}a_2 \quad (2)$$
$$b_3 = S_{31}a_1 + S_{32}a_2 \quad (3)$$
$$b_4 = S_{41}a_1 + S_{42}a_2 \quad (4)$$
$$b_5 = S_{55}a_5 \quad (5)$$
$$b_6 = S_{65}a_5. \quad (6)$$

From (1)–(6), the incident and reflected waves at the HBT (a_2, b_2, a_5, and b_5) can be calculated from the waves measured at the transition analyzer (b_3, b_4, and b_6), according to the following

$$a_2 = (-S_{41}b_3 + S_{31}b_4)/(S_{31}S_{42} - S_{32}S_{41}) \quad (7)$$
$$b_2 = [(S_{21}S_{42} - S_{22}S_{41})b_3 - (S_{21}S_{32} - S_{22}S_{31})b_4]/(S_{31}S_{42} - S_{32}S_{41}) \quad (8)$$
$$a_5 = b_6/S_{65} \quad (9)$$
$$b_5 = (S_{55}/S_{65})b_6. \quad (10)$$

Therefore, the voltage and current waves at the HBT can be calculated according to

$$V_B = \sqrt{Z_0}(a_2 + b_2) \quad (11)$$
$$I_B = (1/\sqrt{Z_0})(a_2 - b_2) \quad (12)$$
$$V_C = \sqrt{Z_0}(a_5 + b_5) \quad (13)$$
$$I_C = (1/\sqrt{Z_0})(a_5 - b_5). \quad (14)$$

Equations (1)–(14) are equally valid for the fundamental and harmonic signals, provided the input and output circuits have been characterized at each harmonic frequency. For practical use, any additional components such as cables, connectors and attenuators are included in the calibration of the input and output circuits, placing Ports 3, 4, and 6 right at the transition analyzer. The attenuators are used to help protect the transition analyzer and to ensure negligible reflection.

With the above calibration procedure, the error of the present technique is mainly dependent on the instrument accuracy. The transition analyzer is estimated to cause an error of 12% and 12° in the magnitude and phase of b_I, respectively. The network analyzer is estimated to cause an error of 3% and 5° in the magnitude and phase of S_{IJ}, respectively. Therefore, the worst-case error is 16% in magnitude and 20° in phase. In practice, the measurement was reproducible to within 5% in magnitude and 7° in phase.

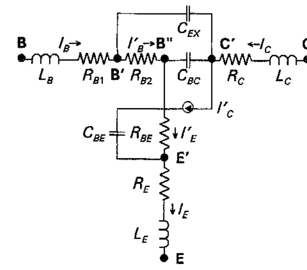

Fig. 3. HBT hybrid-T equivalent circuit. For typical operations with a reverse-biased base-collector junction and without breakdown, the base-collector conduction is negligible. Contact pad capacitances are not considered because calibrated wafer probes are used.

TABLE I
SMALL-SIGNAL MODEL PARAMETERS EXTRACTED FROM S-PARAMETERS $V_{CE} = 2.5V; I_C = 25$ mA

Bias-Independent Parameters	Bias-Dependent Parameters
R_{B1} = 0.49 Ω	R_{BE} = 1.5 Ω
R_C = 0.17 Ω	C_{BE} = 3.1 pF
R_E = 0.79 Ω	C_{EX} = 0.18 pF
L_B = 76 pH	C_{BC} = 0.17 pF
L_C = 78 pH	α_0 = 0.98
L_E = 8 pH	τ_C = 0.5 ps
R_{B2} = 1.9 Ω	

III. HBT MODELING METHOD

The HBT input and output waveforms have been measured under various bias and drive conditions. To extract the intrinsic characteristics from the measured waveforms, it is necessary to extract first the HBT parasitics from bias-dependent S-parameters. As shown in Fig. 3, a hybrid-T equivalent circuit was used in conjunction with a previously developed direct extraction method [9]. Notice that, for typical operations with a reverse-biased base-collector junction and without breakdown, the base-collector conduction is negligible. Contact pad capacitances are not considered because calibrated wafer probes are used. Constant values for terminal resistances and inductances ($R_{B1}, R_C, R_E, L_B, L_C$, and L_E) were obtained from the open-collector S-parameters. The base resistance, as well as the intrinsic and extrinsic base-collector capacitances (R_{B2}, C_{BC}, and C_{EX}) were obtained from the S-parameters under 56 typical bias conditions. Since R_{B2} exhibited little bias dependence, an average value was subsequently used for all biases. C_{BC} and C_{EX}, on the other hand, were fitted to the following formula

$$C_{BC} = [(1-\gamma)/\gamma]C_{EX} \quad (15)$$
$$C_{EX} = c_1 + c_2\sqrt{[(c_3 - I_C)/(c_4 - V_{B'C'})]} \quad (16)$$

where c_1, c_2, c_3, c_3, and γ are fitting constants. B' and C' refer to the HBT internal nodes as indicated in Fig. 3. As an example, Table I lists typical small-signal model parameters for one particular bias point.

Knowing the terminal resistances and inductances, V_B, V_C, and V_E are first transformed into the internal values of V'_B, V'_C, and V'_E, respectively, using standard frequency domain techniques. Next, both the current and voltage waveforms are

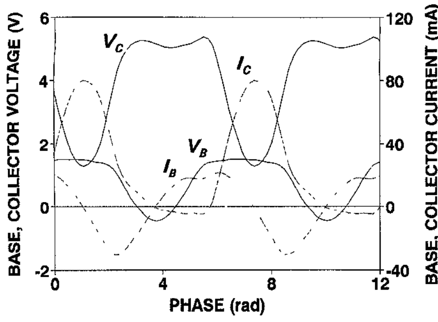

Fig. 4. Measured extrinsic (—) voltage and (...) current waveforms at the base and collector, under a 2 GHz, 11 dBm input drive. A delay of the collector current with respect to the base current is apparent.

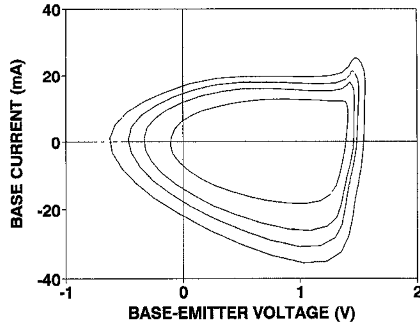

Fig. 5. Measured extrinsic characteristics of base current versus base-emitter voltage. The input power is varied from 8, 10, 11, to 12 dBm. The contours contain large loops, indicating that the displacement current dominates the conduction current due to the base-collector capacitances.

transformed in the time domain into the most intrinsic values, I'_B, V''_B and I'_C according to the following

$$I'B = I_B - C_{EX}\partial V_{B'C'}/\partial t \quad (17)$$

$$V''_B = V'_B - R_{B2}I'_B \quad (18)$$

$$I'_C = I_C + C_{EX}\partial V_{B'C'}/\partial t + C_{BC}\partial V_{B''C'}/\partial t. \quad (19)$$

Equations (15)–(19) can be solved iteratively by first assuming C_{BC} and C_{EX} to be constant. Self-consistent values are usually achieved after one or two iterations. Thus, we can now examine the intrinsic characteristics of the HBT, namely, how I_E changes with $V_{B''E'}$ and how I'_C in turn varies with I_E. By analyzing how I_E changes with $V_{B''E'}, I_E$ can be separated into conduction current (I'_E) and displacement current ($\partial Q_{BE}/\partial t$). Ultimately, the most intrinsic diode characteristics $I'_C(I'_E)$ can be found.

The present results are based on *npn* GaAs/AlGaAs HBT's having an emitter area of approximately 300 μm^2. The current-gain cutoff frequency and the maximum frequency of oscillation are in the range of 30–40 GHz. Details of the HBT design and performance have been described elsewhere [10]. Because the primary purpose of this study is to demonstrate the modeling and characterization techniques, the HBT is conservatively biased Class C with $V_{BE} = 0.8$ V and $V_{CE} = 4$ V. The input drive at 2 GHz was varied from 2–18 dBm. The maximum drive level is approximately 3 dB below saturation.

IV. Results and Discussion

Fig. 4 shows the measured extrinsic waveforms of V_B, I_B, V_C, and I_C under a drive level of 11 dBm. A delay

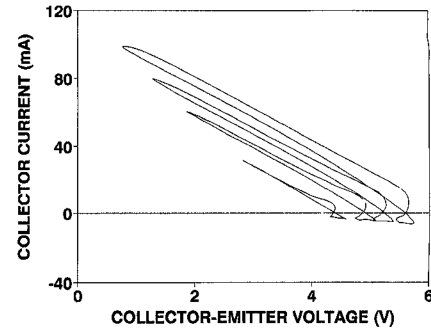

Fig. 6. Measured extrinsic characteristics of collector current versus collector-emitter voltage. The input power is varied from 8, 10, 11, to 12 dBm. The load contours are greatly elongated, reflecting the 50 Ω load impedance of the measurement set up.

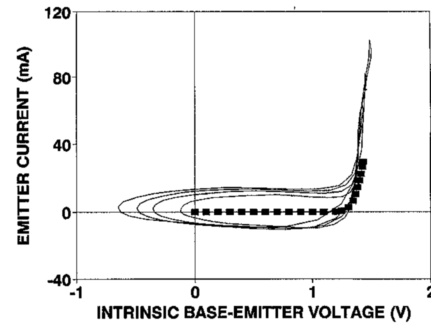

Fig. 7. Measured intrinsic characteristics of emitter current versus base-emitter voltage. The input power is varied from 8, 10, 11, to 12 dBm. The base-emitter characteristics measured at dc is included for comparison. Compared to Fig. 5, Fig. 7 is dominated by diode-like conduction, with only small loops reflecting the intrinsic base-emitter junction capacitance. (—) 2GHz. (■) dc.

of I_C with respect to I_B is apparent. To further visualize how these waveforms are related to each other, Figs. 5 and 6 depict the RF load contours under various drive levels at the base and collector terminals, respectively. It can be seen that the base contours contain large loops, indicating that the displacement current dominates the conduction current due to the base-collector capacitances, thereby masking the intrinsic characteristics of the base-emitter junction. In comparison, the collector contours are greatly elongated, reflecting the 50 Ω load impedance of the measurement set up.

Figs. 7 and 8 show intrinsic contours of $I_E(V_{B''E'})$ and $I'_C(I_E)$, respectively. Compared to Fig. 5, Fig. 7 is dominated by diode-like conduction, with only small loops reflecting the intrinsic base-emitter junction capacitance C_{BE}. In Fig. 8 the contours extend along a 45° slope with increasing drive level. In addition, unlike the extrinsic collector current (Fig. 6), the intrinsic collector current is almost always positive.

If only the conductive part of the emitter current, I'_E, is considered, the contours of $I'_C(I'_E)$ would coalesce into simple lines. Here I'_E is simply taken as the average of I_E between the positive and negative swings at the same $V_{B''E'}$

$$I'_E = [I_E(V_{B''E'}) + I_E(-V_{B''E'})]/2 \quad (20)$$

$$\partial Q_{BE}/\partial t = I_E - I'_E. \quad (21)$$

From this point on, it is relatively straight forward to model the base-emitter current conduction and charge storage in the

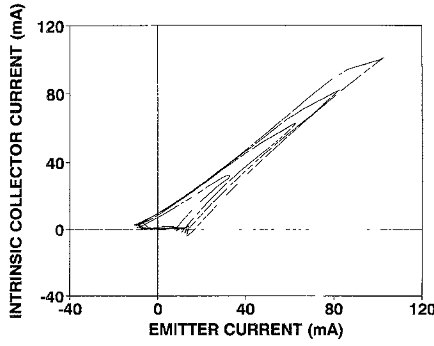

Fig. 8. Measured intrinsic characteristics of collector current versus emitter current. The input power is varied from 8, 10, 11, to 12 dBm. The contours extend along a 45° slope with increasing drive level. In addition, unlike the extrinsic collector current (Fig. 6), the intrinsic collector current is almost always positive.

TABLE II
LARGE-SIGNAL MODEL PARAMETERS EXTRACTED FROM WAVEFORMS

Emitter Conduction Current	Emitter Displacement Current	Collector Conduction Current
$I_F = 1.7\times10^{-19}$ A $n_F = 1.4$ $I_L = 1.2\times10^{-14}$ A $n_L = 2.0$	$C_0 = 0.44$ pF $V_{BI} = 2.0$ V $\tau_B = 0.1$ ps	$\alpha_0 = 0.99$ $I_K = 0.87$ A $\tau_C = 3.2$ ps

time domain. Following the Ebers-Moll model

$$I'_E = I_F[\exp(qV_{B''E'}/n_F kT) - 1] + I_L[\exp(qV_{B''E'}/n_L kT) - 1] \quad (22)$$

$$Q_{BE} = I'_E \tau_B + 2C_0 V_{BI}[1 - \sqrt{(1 - V_{B''E'}/V_{BI})}] \quad (23)$$

where q is the electron charge; k is the Boltzmann constant; T is the absolute temperature; I_F and I_L are the transport and leakage saturation currents, respectively; n_F and n_L are the associated ideality factors; τ_B is a time constant associated with the diffusion capacitance; C_0 is proportional to the depletion space charge; V_{BI} is the built-in voltage of the base-emitter junction. As an example, Table II lists the model parameters extracted from the waveforms measured under an input drive of 11 dBm. The waveforms measured under other input levels gave similar results. The parameter values, while all physically reasonable, offer insights into the HBT operation. For instance, a very small τ_B indicates negligible carrier storage in the base so that the HBT cut-off frequencies are limited by other factors. Fig. 9 shows that the modeled and measured intrinsic base-emitter characteristics agree with each other.

Using (20), the measured $I'_C(I_E)$ can be transformed into $I'_C(I'_E)$ to determine the current gain factor and the collector delay time according to the following

$$I'_C(t) = \alpha_0 I'_E(t - \tau_C)/\{1 + [I'_E(t - \tau_C)/I_K]^2\} \quad (22)$$

where α_0 is the dc current gain factor; τ_C is the collector delay time; I_K specifies the knee point of gain compression as a function of current. These model parameters have also been listed in Table II. Fig. 10 illustrates the excellent fit of

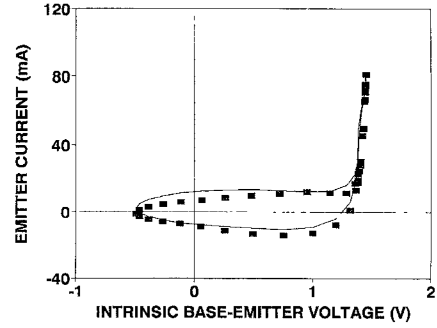

Fig. 9. Agreement between (—) modeled and (■) measured emitter current, for an input power of 11 dBm.

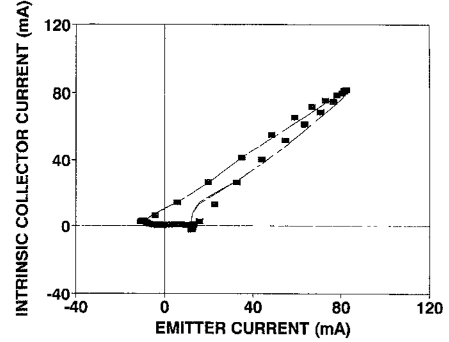

Fig. 10. Agreement between (—) modeled and (■) measured intrinsic collector current as a function of emitter current. Input power = 11 dBm.

the model for the intrinsic collector current as a function of the emitter current.

The above results can be compared with that extracted from dc and small-signal S-parameters in a conventional manner. The base-emitter junction diode characteristics measured at dc has been included in Fig. 7 for comparison. Both the waveforms and the dc characteristics show similar turn-on voltages, but the former rises much steeper than the latter. This is because the base resistances tend to be shunt out by capacitances under RF. In addition, the waveforms cover current values which cannot be measured at dc without burning out the HBT.

Table III compares the delay times extracted from small-signal S-parameters (Table I) and large-signal waveforms (Table II), respectively. In the latter case, the small-signal parameters were derived from the first-order Taylor expansion of large-signal parameters around the same bias point as in the former case. In both cases, the total delay time τ is approximately 5 ps, which consists mainly the collector-transit time τ_C and the base-charging time, $\tau_{RC} = R_{BE}C_{BE}$. However, τ_{RC} dominates in the former case, while τ_C dominates in the latter case. Phenomenologically, since the two models involve a comparable τ, they both can fit the S-parameters at all frequencies. Physically, a longer collector transit time than the base-charging time is more consistent with the structure of a microwave power HBT.

V. CONCLUSION

In conclusion, time-domain waveform characterization has been successfully applied to microwave power HBT's to extract their nonlinear characteristics. Compared to the traditional

TABLE III
TIME CONSTANTS EXTRACTED FROM S-PARAMETERS VERSUS TIME CONSTANTS EXTRACTED FROM WAVEFORMS $V_{CE} = 2.5$ V; $I_C = 25$ mA

Extraction Data Base	Base Charging Time	Base Transit Time	Collector Transit Time	Total Delay Time
S-parameters	4.6 ps	N/A	0.5 ps	5.1 ps
Waveforms	1.2 ps	0.1 ps	3.2 ps	5.3 ps

approach based on dc I-V characteristics and small-signal S-parameters, the present approach is inherently more direct and accurate. It allows insight into the HBT physical operation hence the correct direction for improving the HBT design.

REFERENCES

[1] F. N. Sechi, H. C. Huang, and B. S. Perlman, "Voltage and current waveforms in power MESFETs at microwave frequencies," in *Dig. Int. Solid-State Circuits Conf.,* 1978, pp. 168–169.
[2] M. Sipila, K. Lehtinen, and V. Porra, "High-frequency periodic time domain waveform measurement system," *IEEE Trans. Microwave Theory Tech.,* vol. 36, pp. 1397–1405, Oct. 1988.
[3] G. Kompa and F. van Raay, "Error-corrected large-signal waveform measurement system combining network analyzer and sampling oscilloscope capabilities," *IEEE Trans. Microwave Theory Tech.,* vol. 38, pp. 358–365, Apr. 1990.
[4] F. van Raay and G. Kompa, "A new on-wafer large-signal waveform measurement system with 40 GHz harmonic bandwidth," in *IEEE MTT-S Int. Microwave Symp. Dig.,* 1992, pp. 1435–1438.
[5] C. J. Wei, Y. A. Tkachenko, and J. C. M. Hwang, "Non-invasive waveform probing for nonlinear network analysis," in *IEEE MTT-S Int. Microwave Symp. Dig.,* 1993, pp. 1347–1350.
[6] M. Demmler, P. J. Tasker, and M. Schlechtweg, "A vector corrected high power on-wafer measurement system with a frequency range for the higher harmonics up to 40 GHz," in *European Microwave Conf. Dig.,* 1994.
[7] A. Werthof, F. van Raay, and G. Kompa, "Direct nonlinear FET parameter extraction using large-signal waveform measurements," *IEEE Microwave Guided Wave Lett.,* vol. 3, pp. 130–132, May 1993.
[8] C. J. Wei, Y. Lan, J. C. M. Hwang, W. J. Ho, and J. A. Higgins, "Waveform characterization of microwave power heterojunction bipolar transistors," in *IEEE MTT-S Int. Microwave Symp. Dig.,* May 1995, pp. 1239–1242.
[9] C. J. Wei and J. C. M. Hwang, "New method for direct extraction of HBT equivalent circuit parameters," in *IEEE MTT-S Int. Microwave Symp. Dig.,* May 1994, pp. 1245–1248.
[10] W. J. Ho, N. L. Wang, M. F. Chang, and J. A. Higgins, "Producibility and performance of the microwave power HBT," in *IEEE GaAs IC Symp. Tech. Dig.,* 1992, pp. 263–266.

Ce-Jun Wei (M'93) received the B.S. degree from Qinghua University, China, in 1962 and the Ph.D. degree from Chinese Academy of Sciences in 1966, both in electrical engineering.

From 1966 to 1986, he worked at Chinese Academy of Sciences and was eventually promoted to Full Professor. Between 1980 and 1982, he was also a Visiting Professor at the Technical Institute of Aachen, Germany. Between 1986 and 1988, he was a Visiting Professor at Heinrich-Herz Institute and Berlin Technical University. He joined Lehigh University in 1989 where he is currently Senior Research Scientist of Compound Semiconductor Technology Laboratory. His research interest covers modeling and characterization of microwave devices and circuits, as well as optoelectronics. He has published more than 40 technical papers.

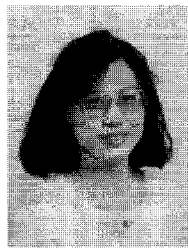

Y. Ellen Lan (S'91–M'95) graduated from Beijing University with the B.S. degree in 1984 and the M.S. degree in 1987, both in physics. From 1989 to 1994, she studied at Lehigh University and received the Ph.D. degree in electrical engineering.

Between 1987 and 1989, she worked on an optical filter for a solar magnetic field detection at Beijing Astronomical Observatory, Chinese Academy of Sciences. She has worked on modeling and characterization of compound semiconductor materials and devices. She has co-authored several technical papers. She is currently with Motorola Phoenix Corporate Research Laboratories at Tempe, Arizona.

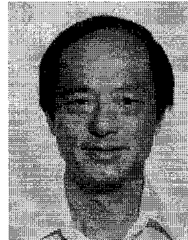

James C. M. Hwang (M'81–SM'82–F'94) graduated from National Taiwan University with a B.S. degree in Physics in 1970. He received the M.S. and Ph.D. degrees in Materials Science and Engineering from Cornell University in 1973 and 1976, respectively.

He had 12 years of industrial experience working at IBM, AT&T, GE, and Gain Electronics. In 1988, he joined Lehigh University as Professor of Electrical Engineering and Director of Compound Semiconductor Technology Laboratory. He has been a consultant for the Air Force Wright Laboratory and the Aerospace Corp. He is a co-founder and director of Quantum Epitaxial Designs, Inc. His interest in compound semiconductors ranges from materials and processing to devices and circuits. He has published over 100 papers and been granted four patents in these areas.

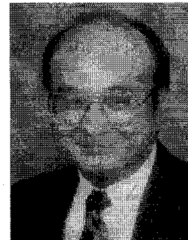

Wu-Jing Ho (M'88) graduated with the B.S. degree in 1973 and the M.S. degree in 1975 from National Tsing Hua University, Taiwan, both in chemistry. He received the Ph.D. degree in materials science from University of Southern California in 1981.

He then worked on advanced silicon devices and GaAs MESFET's until joining Rockwell Science Center in 1986. Since then, he has been active in GaAs- and InP-based HEMT's and HBT's for digital and microwave/millimeter-wave circuits. He participated in transferring the tungsten-silicide-gate MESFET process from IBM to Rockwell. His accomplishments include BiFET LSI technology, multifunctional HBT technology, high-power/high-efficiency HBT MMIC's, high-yield HEMT SRAM's, and HEMT/Schottky-diode IC's. He has over 40 technical publications, one patent, and three patents pending.

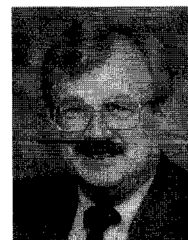

J. Aiden Higgins (M'62–SM'78) graduated with the B.E. (Hons.) degree from Dublin University in 1958. He received the M.S. degree in 1964 and the Ph.D. degree in 1971 from Stanford University, both in electrical engineering.

He joined Rockwell in 1971 where he is currently Manager of the Millimeter-Wave Devices Department at the Science Center. At Rockwell, he led the development of IR detectors and GaAs MESFET's. He pioneered the use of direct ion-implantation and doping-profile tailoring in MESFET fabrication. He was among the first to demonstrate microwave monolithic ICs with active on-chip matching. He designed GaAs CCD's with an agile bandpass filter and a spatial light modulator. He has exploited the use of HEMT's and HBT's for millimeter-wave applications, resulting in state-of-the-art low-noise InGaAs HEMT's and high-power AlGaAs/GaAs HBT's. Currently, his research activities include innovative millimeter wave power combining and packaging. He has over 50 publications and three patents in the area of GaAs devices.